



Supplement of

Airborne bacteria viability and air quality: a protocol to quantitatively investigate the possible correlation by an atmospheric simulation chamber

Virginia Vernocchi et al.

Correspondence to: Federico Mazzei (federico.mazzei@ge.infn.it)

The copyright of individual parts of the supplement might differ from the article licence.

1 **S1: Details on the gas monitors installed at ChAMBRé**

2 The ENVEA-CO12e is a continuous carbon monoxide analyzer based on carbon monoxide detection
3 by infrared light absorption measurement principle (EN 14626:2012, [https://store.uni.com/en/uni-en-
4 14626-2012](https://store.uni.com/en/uni-en-14626-2012)). The concentration of CO in the sample is determined by measuring the quantity of
5 infrared light, at the specific wavelength of 4.67 μm , absorbed by the sample gas as it flows through
6 a multi-reflection chamber. The model available at ChAMBRé also features a built-in module for
7 CO₂ monitoring (range: 0-2000 ppm by NDIR). The instrument has a sampling rate of approximately
8 1 lpm, a response time of 20 s and a detection limit of 0.05 ppm.

9 The measurement principle of ozone by the ENVEA-O342e is based on UV photometry (EN
10 14625:2012 <https://store.uni.com/en/uni-en-14625-2012>). A 254 nm UV light signal is passed
11 through the sample cell where it is absorbed in proportion to the amount of the ozone present
12 (maximum range of ozone absorption 250-270 nm). Periodically, a zero-measurement is
13 automatically performed by the device by switching between the sample stream and a calibrated
14 ozone-free sample. The instrument has a sampling rate of approximately 1 lpm, a response time of
15 20 s and a detection limit of 0.2 ppb.

16
17 The ENVEA-AF22e is based on ultraviolet fluorescence, which is the standard method for the
18 measurement of SO₂ concentrations in ambient air (EN 14212:2012 [https://store.uni.com/en/uni-en-
19 14212-2012](https://store.uni.com/en/uni-en-14212-2012)). A hydrocarbons scrubber guarantees the elimination of hydrocarbon interferences. The
20 hydrocarbons free sample is sent to a reaction chamber to be irradiated by an UV radiation peaked at
21 214 nm, which is the SO₂ molecule absorption wavelength. The fluorescence is optically filtered
22 between 300 and 400 nm to eliminate some interfering gases. With a sampling rate of 0.4 lpm this
23 instrument reaches a detection limit of 0.4 ppb with a response time of 20 s.

24
25 The ENVEA-C32e utilizes the principle of chemiluminescence, which is the standard method for the
26 measurement of NO and NO₂ concentration (EN 14211:2012 [https://store.uni.com/en/uni-en-14211-
27 2012](https://store.uni.com/en/uni-en-14211-2012)), for automatically analyzing the NO-NO_x and NO₂ concentration within a gaseous sample.
28 The analyzer measures the photons emitted after the reaction between NO and O₃. The analyzer
29 initially measures the NO concentration in the sample, through NO ozone oxidation. Subsequently,
30 the sample passes through the heated molybdenum converter, which reduces NO₂ to NO and is then
31 mixed with ozone in the reaction chamber and the resulting NO concentration is determined. In this
32 way, the signal is proportional to the sum of the molecule NO and NO₂ (reduced to NO in the

33 converter) in the sample. With a sampling rate of 0.66 lpm this instrument reaches a detection limit
34 of 0.2 ppb with a response time of 40 s.

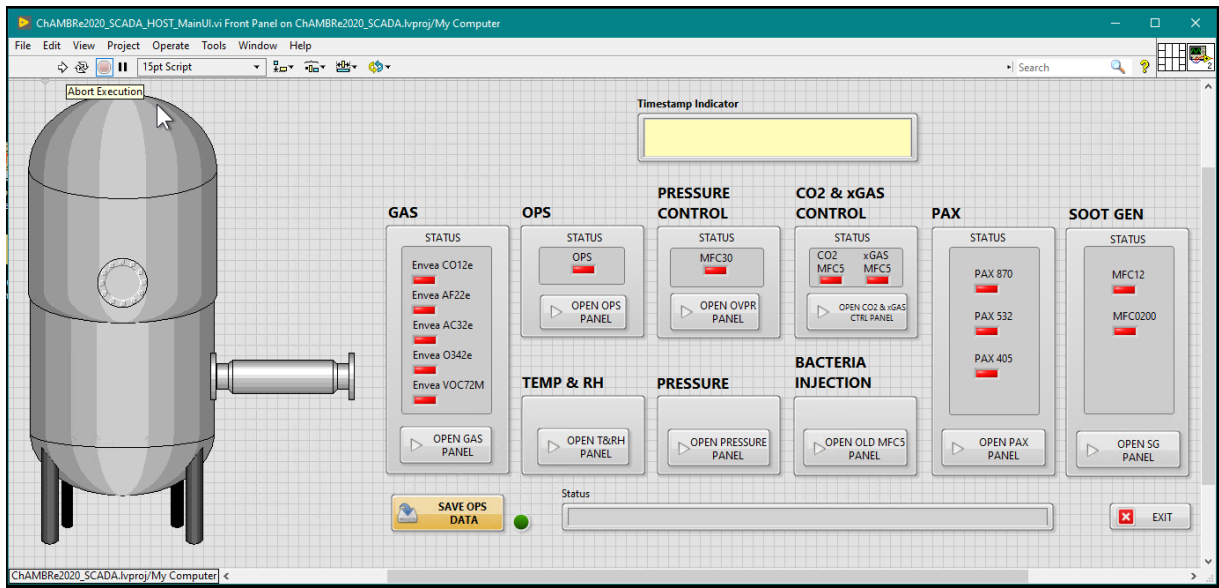
35

36 The ENVEA-VOC72e metrology, in accordance with EN 14662-3 ([https://store.uni.com/en/uni-en-](https://store.uni.com/en/uni-en-14662-3-2015)
37 [14662-3-2015](https://store.uni.com/en/uni-en-14662-3-2015)). The VOC72e performs three main functions: the sampling, the GC analysis and the
38 data processing. The sampling is achieved with a single trap filled with a specific sorbent. Its flow
39 through the trap is about 12 mlpm which gives a sampled volume of 165 ml with the standard 15
40 minutes cycle (sampling time >90% of cycle time). At the end of the sampling cycle, the trap is
41 connected to the GC column and quickly heated from 35 to 380°C within 2 seconds. The compounds
42 are thermally desorbed and flushed with hydrogen into the GC column. Then the trap is cooled with
43 a fan for a new sampling cycle. Inside the GC column, the compounds are moved forward by the
44 hydrogen flow (the mobile phase) and retained by the internal coating (the stationary phase) causing
45 a selective retardation of the compounds. To achieve an optimal separation within a minimal time,
46 the GC column follows a multi slope thermal cycle from a cold step (25°C) for the injection to a hot
47 step (160°C) for flushing all the heavy compounds (i.e., compounds with a high boiling point). At the
48 end of the hot step, the GC column is cooled to the cold step for the next cycle. The GC column
49 output is connected to a photo ionization detector where the compound concentration is converted
50 into a small electric signal. The PID detector includes a 10.6 eV UV lamp that ionizes all the
51 compounds which ionization potential (IP) is less than 10.6 e V. The 240 V electric field between the
52 polarization electrode (-240 V) and the signal electrode (at ground) moves the ionized particles
53 (positive ions and negative electrons) towards the electrodes creating a small electrical conduction.
54 The resulting electric signal is amplified and digitalized in the electrometer board. Its recording gives
55 the chromatogram which exhibits a peak for each detected compound. The standard measured
56 compounds are Benzene, Toluene, Ethylbenzene, m+p-Xylene, o-Xylene, 1-3 Butadiene. Sample
57 flow is around 50 mlpm, with a low detection limit of $\leq 0.05 \mu\text{g m}^{-3}$ (benzene).

58

59 **S2: details on the custom SCADA acquisition and control system developed at ChAMBRé**

60 Figure S1 shows the main graphic user interface (GUI) of the NI LabVIEW custom application
61 running continuously during the experiment. The status (on/off) of each sensor is shown on the main
62 panel by a light indicator. Detailed information about each sensor is available by pressing the related
63 subpanel button. The output data from all sensors are recorded at a user-selectable sampling rate
64 (default: sampling rate = s^{-1}). Time series can be visualized in real-time on the corresponding
65 subpanel. During the experiment the user can also interactively set or modify several sensor
66 parameters via the subpanel controls.



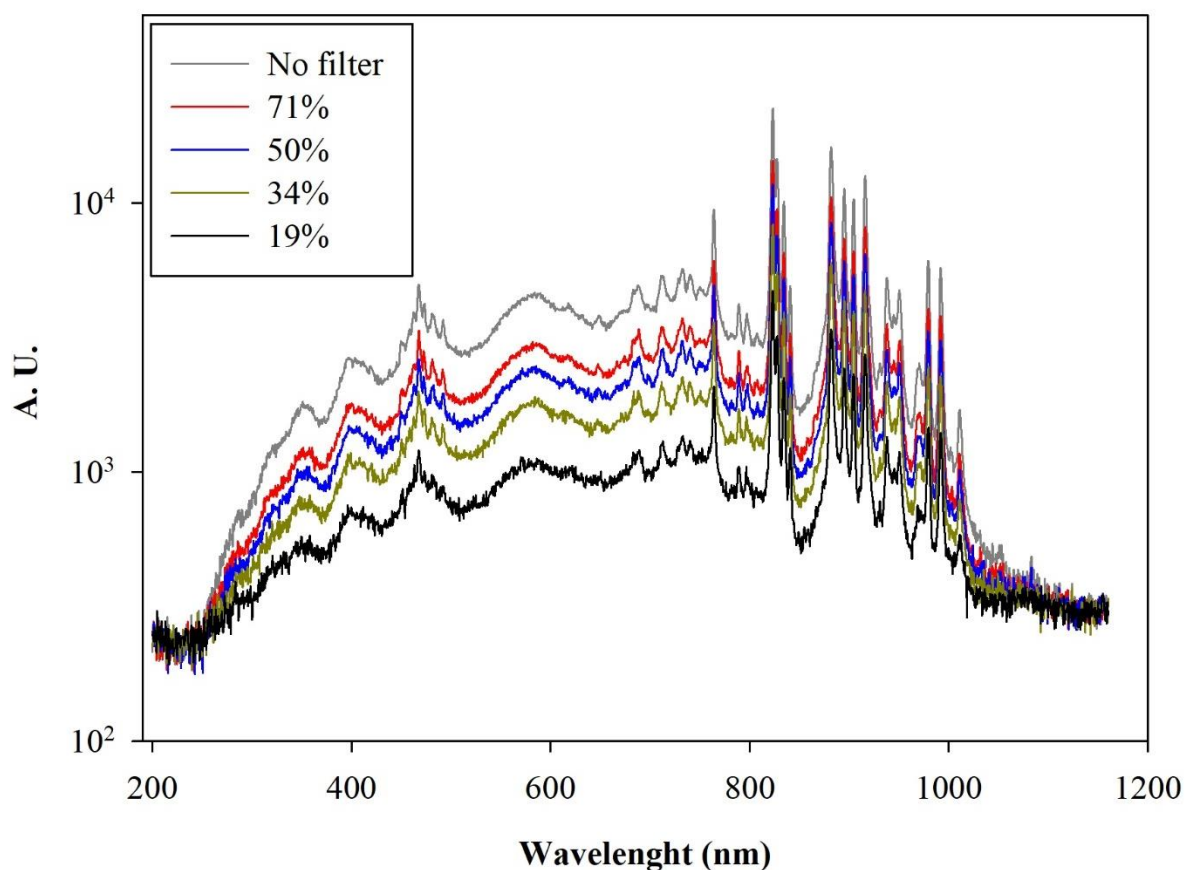
67

68 **Figure S1:** Screenshot of the graphic user interface of the SCADA application developed in LabVIEW™ language.

69

70 **S3: Feature of the Solar Simulator installed at ChAMBR**

71 Several characterization measurements were carried out on the Solar Simulator. The device itself and
 72 its components were tested to assess the performance. Figure S2 shows a comparison of the effect of
 73 the four neutral density filters, which can provide attenuation up to 81% (filter labeled with 19% in
 74 the figure). The spectral features of the light produced by the Solar Simulator remain indeed
 75 unchanged after going through the neutral density filters, with the only appreciable difference being
 76 a uniform attenuation of the transmitted radiation.



77

78 **Figure S2:** Intensity vs wavelength measured with an Avantes ULS2048CL-EVO spectrometer directly at the exit of the
 79 Solar Simulator with and without the available neutral density optical filters. The percentage reported in the legend is the
 80 filter transmittance.

81

82 The stability of the Solar simulator has been measured over a period of 6 hours, resulting in a
 83 maximum deviation (actually increase) of 6% in light intensity, likely due to the warming up of the
 84 solar simulator lamp which takes nominally 20 minutes, but it is also subjected to small fluctuation
 85 linked to the surrounding environmental conditions.

86

87 **S4: *E. coli* growth curve**

88

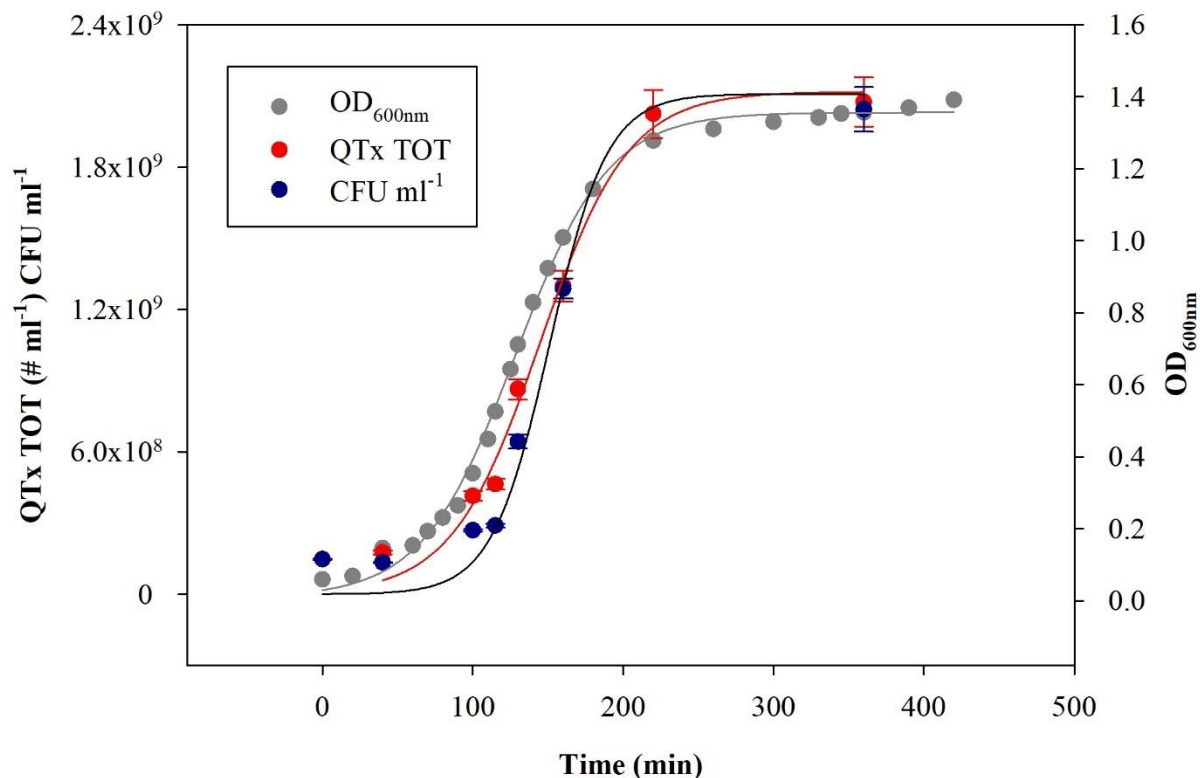
89 Bacterial growth is a complex process that involves several distinct phases. The increase in numbers
 90 or bacterial mass can be measured as a function of time under culture conditions where the nutrients
 91 and environmental conditions are controlled. Several distinct growth phases can be observed within
 92 a growth curve such as the lag phase, the exponential or log phase, the stationary phase, and the death
 93 phase. The first stage, the lag phase, occurs when bacteria are not dividing but are metabolically
 94 active. During the lag phase of the bacterial growth cycle, the synthesis of RNA, enzymes, and other

95 molecules occurs. The length of this phase depends on the type of bacterial species, culture medium,
96 and environmental factors. The log phase is an exponential phase characterized by rapid growth, with
97 binary fission. The number of new bacteria appearing per unit time is proportional to the present
98 population. If growth is not limited, doubling will continue at a constant rate, so both the number of
99 cells and the rate of population increase doubles with each consecutive period. Exponential growth
100 cannot continue indefinitely, however, because the medium is soon depleted of nutrients and enriched
101 with catabolites. The stationary phase is due to a growth-limiting factor; this is mostly depletion of a
102 nutrient, and/or the formation of inhibitory products such as organic acids. Instead during the death
103 phase, the number of living cells decreases exponentially. Bacteria run out of nutrients and die
104 although the number of cells stays constant. The decline phase is brought by exhaustion of nutrients,
105 accumulation of toxic products, and autolytic enzymes. The microbial growth curve is a record of the
106 countable cells determined at certain time intervals during the population's evolution. In our work,
107 the calibration curve was figured out converting the rate growth from optical density (OD) values to
108 CFU (Colony Forming Unit) ml⁻¹, as explained in detail below.

109 The day before the experiment, bacteria cells are scraped off agar medium, where they are cultivated,
110 using sterile plastic loops and suspended in a sterile, non-selective culture broth medium Tryptic Soy
111 Broth (TSB) and incubated overnight at 37 °C. The day after, 3 ml of the bacteria culture is diluted
112 in 30 ml of new broth medium, and the suspension is incubated again at 37 °C. At intervals of about
113 thirty minutes, the OD of the bacterial solution is measured by the spectrophotometer at $\lambda = 600 \text{ nm}$;
114 $\text{OD}_{600\text{nm}}$ allows to estimate the concentration of bacterial cells in the liquid and tracking the growth.
115 The mid-exponential phase is typically reached when $\text{OD}_{600\text{nm}}$ is about 0.5 (Mytilinaios et al., 2012;
116 Hall et al., 2014). For selected OD values, the bacterial concentration was also measured/referred as
117 Colony Forming Units (CFU). The bacteria solution must be diluted several times to obtain not
118 overlapping colonies on Petri Dishes: 100 μl of bacterial solution is added in 900 μl of sterile saline
119 solution (NaCl 0.9 %), then diluted again as many times as the theoretical concentration (calculated
120 using the OD value) required; 100 μl of the last dilution is spread in duplicate on an TSB agar and
121 incubated overnight at 37 °C. The next day the concentration of culturable cells is measured by
122 counting the colonies formed and multiplying by the proper dilution factor to retrieve CFU
123 concentration in the original solution. Data, obtained by CFU counting on agar plates, are weighted
124 averaged and used to figure out the uncertainty (standard error of weighted mean) of the bacterial
125 concentration in the solution. The weights are the relative uncertainties of CFU number on agar plates
126 following the Poisson statistics.

127 We followed the growth of *E. coli* in suspension culture for about 8 hours from lag phase to horizontal
 128 asymptote and the OD_{600nm}, the total number of *E. coli* (QTx TOT), measured with Quantum TX and
 129 the CFU ml⁻¹ values are reported in Figure S3.

130



131

132 **Figure S3:** Grow curve for *E. coli*: optical density (OD_{600nm}), total number of *E. coli* measured by QUANTOM-TX (#
 133 ml⁻¹) and the corresponding bacteria concentration (CFU ml⁻¹) vs. time. Error bars have, in most cases, the same size of
 134 the data points and they are calculated as previously described.

135

136 **S5: details on the procedure to the optimum setting of the Quantum Tx counter**

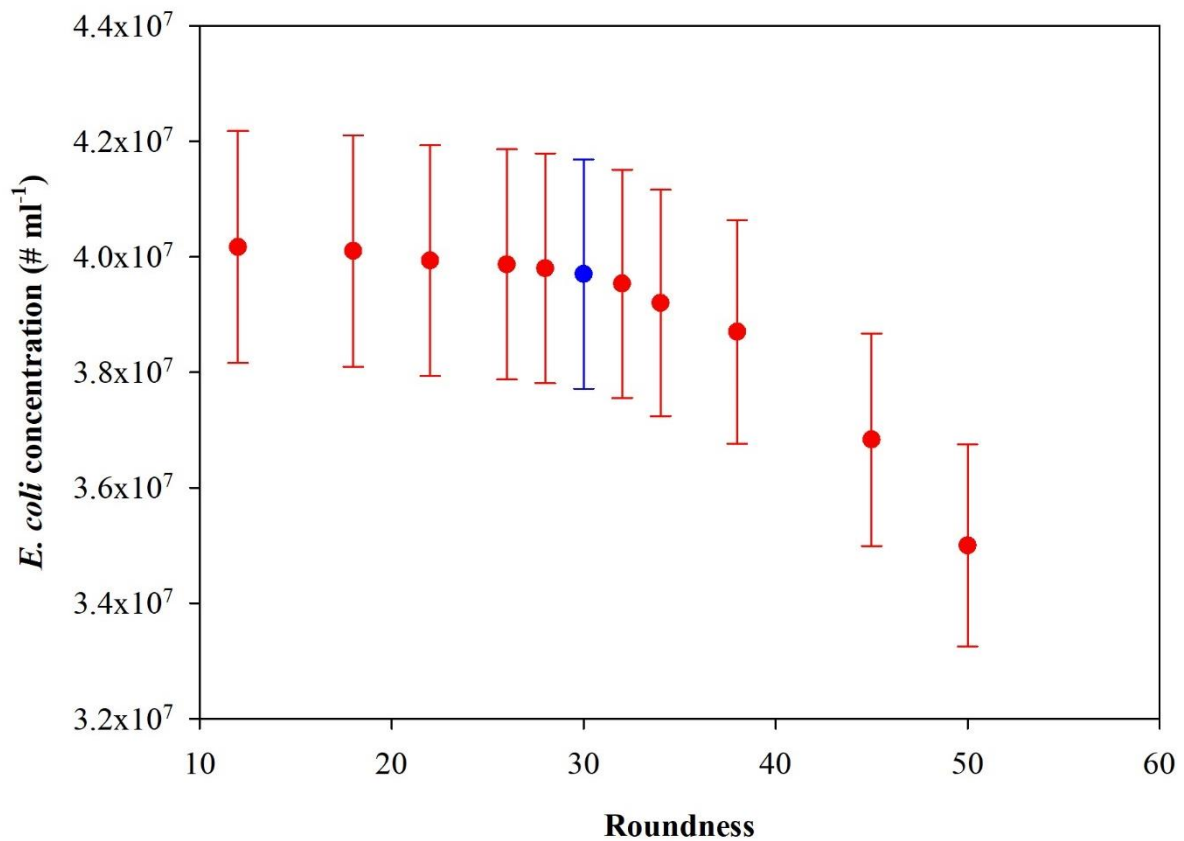
137 The Quantum Tx has a factory standard counting protocol already preset, but several parameters must
 138 be tuned on the characteristics of different bacterial species: Table S.1 reports the counting parameters
 139 and the suggested factory settings for *E. coli*.

140

141 **Table S1:** Quantum Tx factory setting suggested for optimal counting for *E. coli*.

Parameter	Range	Default	<i>E. coli</i>
Dilution factor	1-20000	2	2
Min Fluorescent object size (µm)	0.3-49	0.3	1
Max Fluorescent object size (µm)	0.4-50	50	50
Roundness (%)	0-100	30	30
De-clustering level	0-10	7	7

	Detection sensitivity	0-9	4	3
142				
143	The <i>Dilution factor</i> must be set before counting and it is the ratio between the final volume of the			
144	sample (bacterial suspension + reagents) and the volume of the bacterial suspension.			
145	The <i>Fluorescent object size</i> measures the diameter of the fluorescent signal from the nucleic acid			
146	stains. This does not correspond to the physical size of the cell. For the bacterial strain, used in our			
147	experiments, the counts of fluorescent signals should be between 1 and 50 μm . <i>Roundness</i> selects			
148	cells based on their shape: the counting algorithm includes objects that are less round at lower values.			
149	Higher values include rounder shapes. The <i>De-clustering</i> function allows for the efficient detection			
150	of cells that may grow in clusters or chains. Higher values will lead to a higher sensitivity to clusters.			
151	The last parameter, <i>Detection sensitivity</i> refers to the sensitivity of fluorescence detection. Higher			
152	values detect fainter signals from weakly stained cells or smaller sample sizes but can also increase			
153	noise. In our experiments, various measurements were made by raising and lowering the <i>Roundness</i> ,			
154	<i>De-clustering level</i> and <i>Detection sensitivity</i> parameters to verify if the standard protocol was optimal.			
155	Below, the trend of <i>E. coli</i> bacterial concentration, varying the three parameters described above, is			
156	shown. The <i>E. coli</i> concentration curve as a function of <i>Roundness</i> parameter shows a flat trend up			
157	to a value of about 40% and then decreases rapidly for higher values: <i>E. coli</i> is a rod shape so high			
158	<i>Roundness</i> values (i.e., sphericity of the object) lead to an underestimation of the total count.			
159				

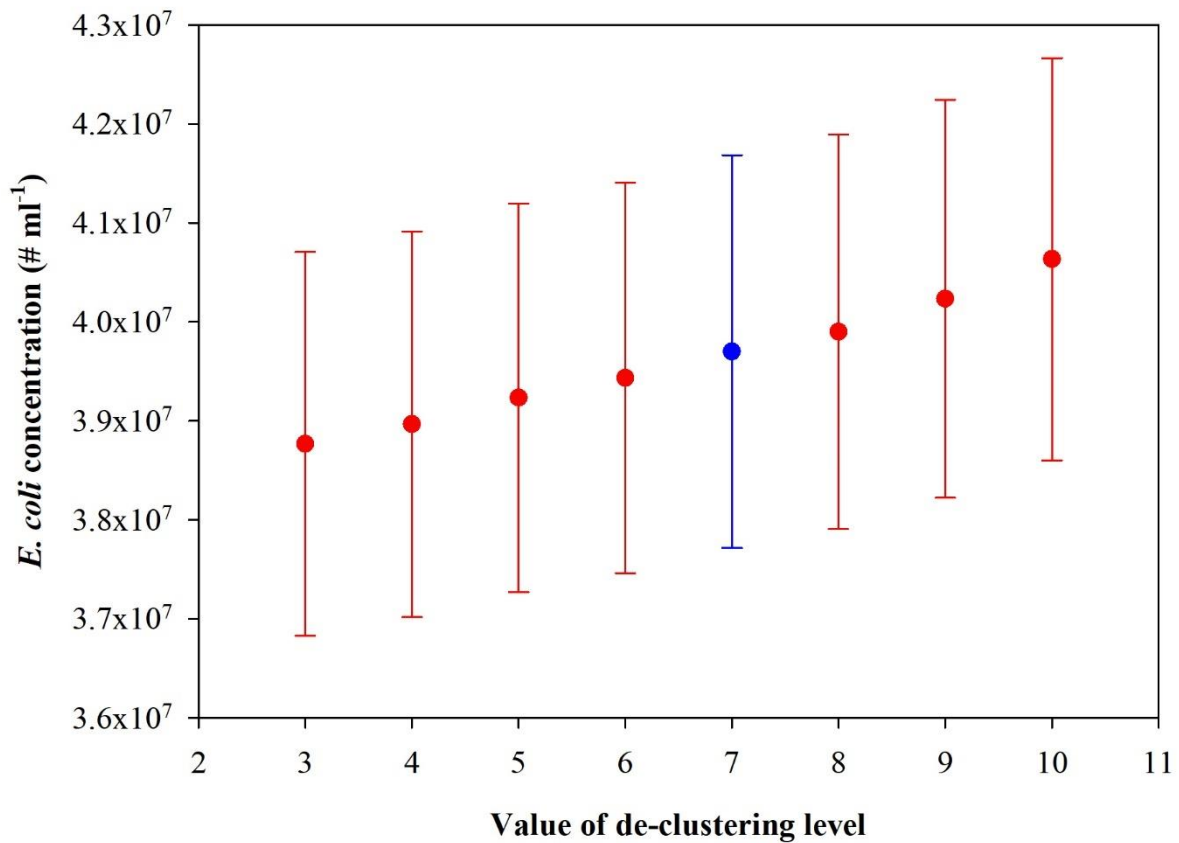


160

161 **Figure S4:** Trend of the *E. coli* concentration as a function of the change of the "Roundness" parameter. The point in blue
 162 is the value obtained following the standard protocol for *E. coli*.

163

164 Figure S5 shows that the value of the bacterial concentration is not dependent on the variation of the
 165 *De-clustering level*; this is probably because the images analyzed didn't show large agglomerations
 166 or clusters. Anyway, raising this parameter, the count of bacterial concentration could increase due
 167 to the ability of the instrument to separate clusters and individual components. However, it is worth
 168 remembering that the clusters are usually probe agglomerates and, therefore, high value of *De-*
 169 *clustering level*, could lead to include non-bacterial cells in the count.



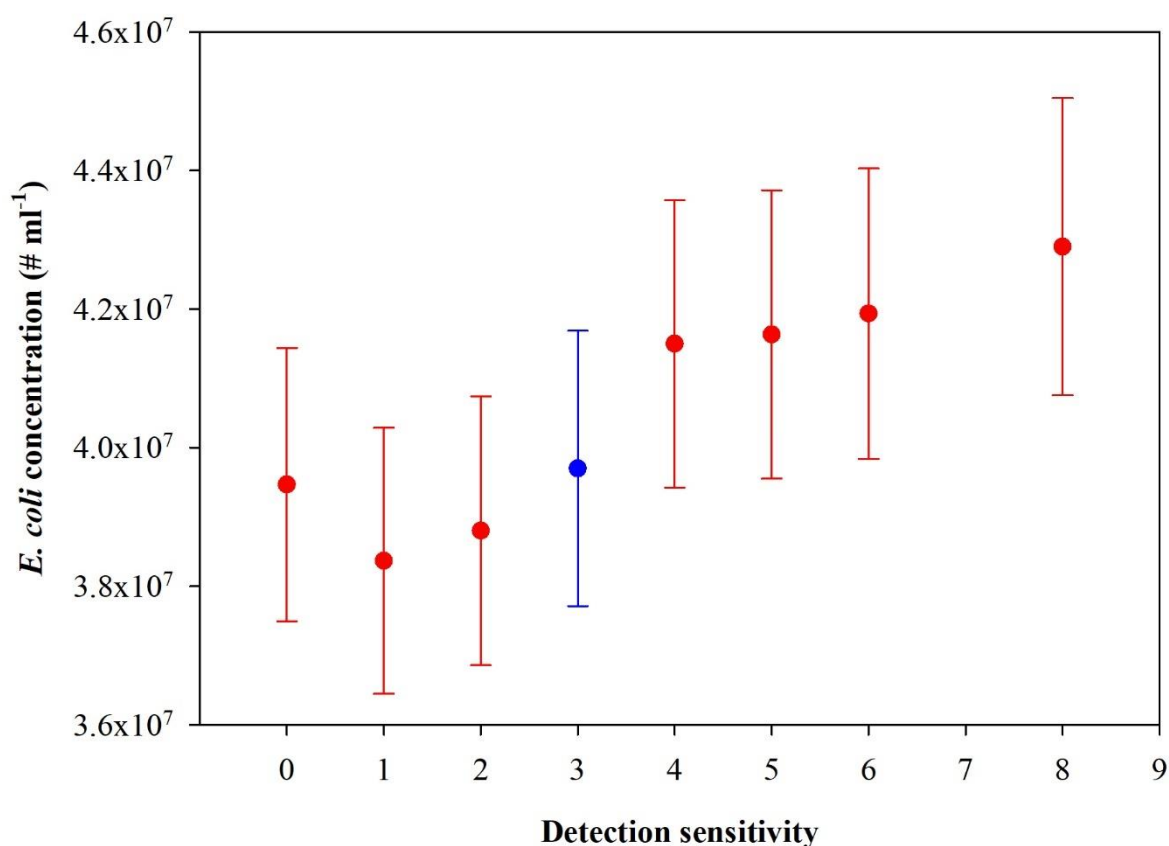
170

171 **Figure S5:** Trend of the *E. coli* concentration as a function of the change of the "De-clustering level" parameter. The
 172 point in blue is the value obtained following the standard protocol for *E. coli*.

173

174 The *E. coli* concentration vs. *Detection sensitivity* shows the same trend as before; it is a flat curve as
 175 the value of detection sensitivity changes. However, it is not recommended to select the lower or
 176 higher value of detection sensitivity since some *E. coli* could be lost in the total count or the
 177 background noise could increase, decreasing the quality of the images captured by the instrument,
 178 respectively.

179



180

181 **Figure S6:** Trend of the *E. coli* concentration as a function of the change of the "Detection sensitivity" parameter. The
 182 point in blue is the value obtained following the standard protocol for *E. coli*.

183

184 The results of these experiments showed that the variation of *Roundness*, *De-clustering level* and
 185 *Detection sensitivity* does not affect the total bacteria concentration count (except for higher value of
 186 *Roundness*) and the default protocol, suggested by the manufacturer, can be used without additional
 187 adjustments.

188

189 **S6: reduction of *E. coli* viability measured in a set of experiments at ChAMBRé**

190

191 The experimental protocol discussed in the article is based on the monitoring, during the exposure to
 192 the ChAMBRé atmosphere, of the concentration of viable bacteria by active sampling with a single-
 193 stage Andersen impactor. The optimum sampling time to collect on the petri dishes in the impactor
 194 a well countable number of bacteria (i.e., between 30 and 150 CFUs) while avoiding diluting too
 195 much their concentration in the chamber was thoroughly investigated. During the experiment such
 196 sampling time necessarily changes to consider the quite fast reduction of the bacteria (*E. coli*)
 197 viability. Results are given in Table S2.

198 **Table S2:** Sampling time set for the Andersen impactor during the *E. coli* experiments for different time (in minute) after
 199 the injection of bacteria.

Experiment	t: 0	t: 30	t: 60	t: 90	t: 120
Baseline dark	5 sec	10 sec	30 sec	1 min	1 min
NO ₂ (900 ppb)	5 sec	30 sec	1 min	2 min	2 min
NO ₂ (1200 ppb)	5 sec	30 sec	2 min	2 min	3 min
NO (900 ppb)	5 sec	30 sec	1 min	2 min	2 min
NO (1200 ppb)	5 sec	30 sec	1 min	2 min	2 min
Baseline light	5 sec	30 sec	1 min	2 min	2 min

200

201 Reduction in *E. coli* viability over time and with the ChAMBR_e volume filled with a constant
 202 concentration of a single pollutant are reported in Table S3. In all cases, the chamber was maintained
 203 in darkness.

204

205 **Table S3:** Ratio of bacteria viable concentration during pollutants experiments and baseline experiments. Values indicate
 206 the V:T ratio with pollutant and in the baseline experiment.

POLLUTANT (ppb)	Time after injection (min)				
	0	30	60	90	120
O ₃ (>1000)	0.15 ± 0.06	0	0	0	0
NO ₂ (900)	0.71 ± 0.19	0.37 ± 0.06	0.29 ± 0.05	0.14 ± 0.06	0.08 ± 0.03
NO ₂ (1200)	0.37 ± 0.13	0.03 ± 0.01	0.01 ± 0.01	0.04 ± 0.03	0.01 ± 0.02
NO (900)	0.36 ± 0.12	0.13 ± 0.03	0.23 ± 0.04	0.47 ± 0.12	0.24 ± 0.07
NO (1200)	0.58 ± 0.19	0.25 ± 0.04	0.30 ± 0.05	0.45 ± 0.14	0.10 ± 0.04

207

208 **References**

209 Hall, B. G., Acar, H., Nandipati, A., Barlow, M.: Growth Rates Made Easy, *Mol. Biol. Evol.* 31, 232–
 210 238, <https://doi.org/10.1093/molbev/mst187>, 2014.

211 Mytilinaios, I., Salih, M., Schofield, H. K., Lambert, R. J. W.: Growth curve prediction from optical
 212 density data, *Int. J. Food Microbiol.* 154, 169–176,
 213 <https://doi.org/10.1016/j.ijfoodmicro.2011.12.035>, 2012.

214